Materials Science & Engineering A 676 (2016) 271–277

Contents lists available at ScienceDirect

Materials Science & Engineering A

journal homepage: www.elsevier.com/locate/msea

Time-of-Flight Secondary Ion Mass Spectrometry (ToF-SIMS) imaging of deuterium assisted cracking in a 2205 duplex stainless steel microstructure

Oded Sobol [a], Gerald Holzlechner [a], Gert Nolze [a], Thomas Wirth [a], Dan Eliezer [b], Thomas Boellinghaus [a,*], Wolfgang E.S. Unger [a]

[a] BAM – Federal Institute for Materials Research and Testing, Berlin, Germany
[b] Department of Materials Engineering, Ben-Gurion University of the Negev, Beer Sheva, Israel

ARTICLE INFO

Article history:
Received 20 June 2016
Received in revised form
26 August 2016
Accepted 27 August 2016
Available online 30 August 2016

Keywords:
Hydrogen assisted cracking
Hydrogen embrittlement
ToF-SIMS
SEM
FIB
EBSD

ABSTRACT

In the present work, the influence of deuterium on the microstructure of a duplex stainless steel type EN 1.4462 has been characterized by Time-of-Flight Secondary Ion Mass Spectrometry (ToF-SIMS) supported by scanning electron microscopy (SEM), focused ion beam (FIB), electron back scattered diffraction (EBSD) and energy dispersive x-ray (EDX) investigations. Characterization has been carried out before and after electrochemical charging with deuterium which has been used as a tracer, due to its similar behavior to hydrogen in the steel microstructure. In a first approach, the distribution of the deuterium occurring at temperatures above −58 °C has been visualized. Further it turned out that sub-surface micro blisters are formed in the ferrite-austenite interface, followed by the formation of needle shaped plates and subsequent cracking at the ferrite surface. In the austenite phase, parallel cracking alongside twins and hexagonal close packed (martensitic) regions has been observed. In both phases and even in the apparent interface, cracking has been associated with high deuterium concentrations, as compared to the surrounding undamaged microstructure. Sub-surface blistering in the ferrite has to be attributed to the accumulation and recombination of deuterium at the ferrite-austenite interface underneath the respective ferrite grains and after fast diffusing through this phase. Generally, the present application of chemometric imaging and structural analyses allows characterization of hydrogen assisted degradation at a sub-micron lateral resolution.

1. Introduction

Duplex stainless steels (DSS) are widely applied in many industrial branches for several decades, in particular in the chemical and petro-chemical area, due to their excellent combination of properties, as for instance a considerable strength and ductility combination as well as improved localized and stress corrosion resistance at a good weldability [1]. Duplex stainless steels consist of a ferritic-austenitic microstructure with both phases present in significant portions. Specifically, the widely applied alloy DSS 2205 (EN 1.4462, UNS S31803) with about 22 Cr, 5 Ni and 3 Mo (wt.-%) consists of about 50 vol% face centered cubic (FCC) austenite islands in base centered cubic (BCC) ferrite. In wrought components the DSS microstructure shows a rolling texture due to hot working and subsequent solution annealing [2]. In the recent years, Lean Duplex Stainless Steels (LDSS) with a lowered alloying content are gaining increasing importance, due to an even better cost-property relation. As additional two-phased steel types, i.e. martensitic-austenitic alloys are drawn increasingly into research focus, in particular due to their improved deformation-absorbing capacities.

However, as evidently shown by several failure cases in the past, DSS is prone to hydrogen assisted cracking (HAC), since hydrogen might interact with the microstructure, degrade the mechanical properties, respectively, and even initiate various microstructural changes in such alloys [3–5]. Also, the interface between the phases is frequently anticipated as trapping site for hydrogen and, especially, the different solubility and diffusibility of hydrogen in the two phases contributes to the HAC-susceptibility of these steels [6,7].

Remarkable attempts have been made in the past to analyze permeation, effusion and distribution of hydrogen (and deuterium) together with respective degradation phenomena in duplex

* Corresponding author.
E-mail address: thomas.boellinghaus@bam.de (T. Boellinghaus).

http://dx.doi.org/10.1016/j.msea.2016.08.107
0921-5093/

stainless steels [8]. Such phenomena are subjected to microstructural changes in both, the austenite (γ) and ferrite (δ) phase. In the ferrite, a strong increase of the dislocation density has been observed to be associated with increasing hydrogen concentrations [9]. In the austenite, the density of stacking faults grows with the hydrogen concentration [10]. Moreover, at increasing hydrogen concentrations due to cathodic charging, a martensitic phase transformation might occur [10]. However, the mechanisms behind the interactions between hydrogen and the respective phases in duplex stainless are not yet completely understood. An example that demonstrates the importance of metallurgical phenomena associated with hydrogen assisted cracking (HAC) in stainless steels has been given by Szummer et al. [11]. These authors report multiple twinning caused by hydrogen which becomes visible as grain oriented needle shape features on the surface. In addition, they observed that increasing of the dislocation density and microhardness may lead to the formation of micro-cracks. The authors also concluded that during hydrogen diffusion in the steel, the respective concentration in the near surface zone is much higher in comparison to the bulk. Głowacka et al. [10] confirmed different influences of hydrogen on the phase specific microstructure in a typical 2205 alloy by application of scanning electron microscopy (SEM) and electron back-scattered diffraction (EBSD). They particularly clarified phase transformations assisted by hydrogen. As another feature, a strong increase of dislocation density has been detected in the ferrite phase [10]. During longer hydrogen charging times also twin were formed in the ferrite phase. In the austenitic phase, it has been observed that the generation of stacking faults was followed by the formation of α′ martensite [10]. In summary, the literature shows a detailed understanding of HAC in DSS is of high technological interest. The knowledge-gaps about real hydrogen-microstructure interactions and the metallurgical mechanisms behind HAC have also to be attributed to a lack of imaging techniques for monitoring and elucidating hydrogen locally at sub-micron lateral resolution [5].

In the past few years, Time-of-Flight Secondary Ion Mass Spectrometry (ToF-SIMS) has been shown to be a powerful tool to precisely map the distribution of hydrogen, along with other elements, in steel microstructures [8,12–14], delivering data from the very surface (with a surface sensitivity below 1 nm) [15]. In addition to a literature survey on SIMS experiments related to hydrogen effects given elsewhere by the authors [12], highly resolved imaging examples are shown by Tarzimoghadam et al. [13] who utilized SIMS for the investigations of hydrogen assisted degradation in a Ni based superalloy. Awane [16] studied hydrogen diffusion profiles in an austenitic stainless steel at room temperature by SIMS sputter depth profiling. Nishimoto et al. [17] detected hydrogen in the ferritic grains by SIMS using a cryogenic sample holder. State-of-the-art ToF-SIMS instruments may provide precise element and phase mappings with a lateral resolution below 100 nm [18], enabling imaging of the microstructure and analysis of its phase dependent chemical composition [13,14,19]. Recently, ToF-SIMS image analysis has substantially been improved by multivariate analysis (MVA) of image data and by data fusion of the chemical and topographic information [14]. For these reasons, ToF-SIMS as the primary analysis tool used has been combined with high resolution scanning electron microscopy (HRSEM).

The study and the results reported here have been targeted at new insights into hydrogen assisted degradation and cracking mechanisms in multiphase microstructures, exemplified at a typical DSS. Since the hydrogen distribution in the respective microstructure can usually not be differentiated from hydrogen adsorbed from the rest gas in the analysis chamber of the ToF-SIMS instrument and thus, to avoid confusions about the origin of the measured hydrogen, the specimens investigated in this study have been electrochemically charged with deuterium. It has to be emphasized, however, that deuterium behaves similarly to hydrogen in metallic microstructures [13,20,21]. With respect to hydrogen embrittlement (HE), deuterium is commonly used as a tracer of hydrogen in analyses of metals by methods such as ToF-SIMS [13,22–24]. The approximate diffusion coefficients for hydrogen in the duplex microstructure are $D_\delta \approx 1.5_X10^{-11}$ m^2/s for ferrite and $D_\gamma \approx 1.4_X10^{-16}$ m^2/s for austenite [25]. Most authors assume that hydrogen and deuterium are not differing qualitatively but quantitatively because of the isotopic mass effect. The ratio between the diffusion coefficients for hydrogen (D_H) and deuterium (D_D) equals to the inverse ratio of the square root of the isotopic masses [22,23]. Johnson et al. [26] showed experimentally that for iron this ratio is 1.8 for both permeability (Φ_H/Φ_D) and diffusivity (D_H/D_D).

2. Experimental

2.1. Sample preparation and electrochemical charging

The raw material was purchased from ThyssenKrupp and specified by Edelstahlwerke GmbH (chemical composition specified by the supplier is given in Table 1). The as-received material was in the form of a rod after solution-annealing at 1050 °C and water quenching with a measured ferrite content of 51 vol%. Small samples ($13 \times 9 \times 1.0$ mm^3) were prepared by spark cutting and carefully grinded and polished using a 0.25 μm diamond suspension as the final step. Before charging with deuterium, all samples were cleaned for 10 min in an isopropanol ultrasonic bath. Electrochemical charging with deuterium was carried out galvanostatically in a solution of 0.05 M D_2SO_4 and 0.01 M $NaAsO_2$ acting as a recombination poison at a current density of 5 mA/cm^2. Samples were charged between 72 h and 168 h. To reduce rapid effusion of deuterium, the samples were immediately externally cooled and subsequently mounted on a cooling device after charging and then conveyed into the ToF-SIMS instrument airlock chamber.

2.2. Time-of-Flight Secondary Ion Mass Spectrometry (ToF-SIMS)

After external cooling to −70 °C the sample was transferred through the sample lock into the ToF-SIMS analysis chamber where it was further cooled down to −120 °C. The measurements were carried out on a TOF-SIMS IV instrument (ION-TOF GmbH, Muenster, Germany). A pulsed bismuth primary ion gun (25 keV, Bi_3^{++}) was used in the "collimated burst alignment" (CBA) mode enabling high lateral resolutions below 100 nm [18,27]. Additionally, to ToF-SIMS imaging in the CBA mode, high mass resolution spectra were acquired using the high current bunched mode (HCBU) to differentiate contributions of H_2^- and D^- and OH_2^- and OD^- secondary ions (SI) to the peaks at $m/z=2$ and $m/z=18$, respectively. To remove surface contaminations from the sample and for co-sputtering during analysis, an area of 450×450 μm^2 was sputtered with a 3 keV Cs^+ beam. The sputter time was 5 min for surface cleaning and 1 min for co-sputtering after every data acquisition. Cs^+ co-sputtering was used to enhance the negatively charged secondary ion yield [14]. Imaging of the deuterium distribution was carried out by scanning a field-of-

Table 1
Chemical composition of the 2205 duplex stainless steel delivered by the supplier (wt%).

C	Cr	Ni	Mo	Mn	N	Fe
0.018	22.35	5.54	3.08	1.82	0.156	Balanced

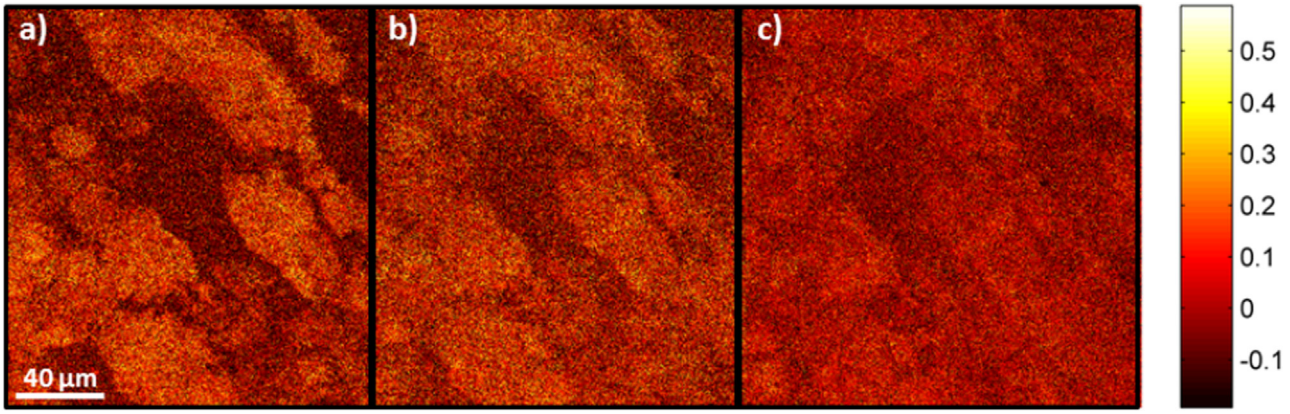

Fig. 1. PC1 loading plots taken from the same area during sample warm-up of a DSS sample charged for 72 h: (a) −96 °C to −60 °C, (b) −58 °C to −30 °C, (c) −29 °C to −4 °C. PC1 is representative for deuterium in the microstructure. The distribution of deuterium in the microstructure becomes visible as a blurring of the interfaces between the phases when temperature increases. (a) suggests that at low temperature the deuterium is captured in the austenite phase and that the effusion and migration to the ferrite is rather slow, (b) shows the deuterium diffusion from the austenite 'reservoir' into the ferrite, and (c) indicates the loss of deuterium in the sample when the sample is approaching room temperature.

view of $100 \times 100\ \mu m^2$ with 1024×1024 or 512×512 pixels and $30 \times 30\ \mu m^2$ with 256×256 pixels for high resolution images. Imaging for phase distinction has been made in the positive mode with the sample at room temperature. To enhance the metal secondary ion yields, the sample was sputtered with O_2 primary ions for 1 min. Finally, ion induced secondary electron (SE) images were acquired to enable analysis of the same field-of-view with the SEM later.

2.3. Scanning Electron Microscopy (SEM), Energy Dispersive X-ray Spectroscopy (EDS) and Electron Back Scattered Diffraction (EBSD)

Once SIMS analyses had been finished, the samples have been investigated with SEM. High resolution images were acquired by a Zeiss Supra 40 instrument (Carl Zeiss, Oberkochen, Germany) equipped with a Schottky field emitter and having attached a silicon drift detector (SDD). The micrographs were recorded with an Everhart-Thornley detector using 10–20 kV. EDX measurements have been taken in 15 kV by a Thermo Fisher Scientific (Waltham, MA, USA) detector with a 100 mm^2 area and a resolution of 512×384 pixels (140pA, 6 s). EBSD has been carried out for respective phase transformation characterizations to be attributed to deuterium (hydrogen) charging. EBSD investigations were performed in a field emission scanning electron microscope (FE-SEM) LEO Gemini 1530VP FE-SEM (Carl Zeiss, Oberkochen, Germany) with an attached EBSD system of Bruker Nano. EBSD patterns were acquired by an e^-Flash^{HR} system equipped with back- and forescattered electron detectors (ARGUS) with a resolution of 160×120 pixels. The diffraction patterns were collected using 20 kV, a beam current of about 12 nA, step size of 380 nm and a dwell time of 15 ms. 6 of 12 bands were correctly indexed. The data processing was carried out using CrystAlign (ESPRIT, Bruker Nano, Berlin). EBSD phase maps were acquired from the same area before and after electrochemical charging with deuterium. The samples were grinded and polished with colloidal silica and then charged for 72–96 h with identical charging parameters to the ones described for the ToF-SIMS analyses (Section 2.1).

2.4. Principle Component Analysis (PCA) and data fusion

Raw ToF-SIMS imaging data have been treated with Principal Component Analysis (PCA). Using PCA enables that all the deuterium related information in the mass spectra (e.g., D^-, OD^-, CrD^-) can be utilized for visualization of the deuterium distribution as the first Principle Component (PC1). This leads to an improved contrast and, consequently, to more details in the image. Later, the HRSEM and PCA treated ToF-SIMS image data have been fused. Data treatment for PCA and data fusion was made using the ImageLab software (v1.02, EPINA, Pressbaum, Austria). Prior to PCA, the raw data have been pre-processed by normalizing the secondary ions to the total intensity of each respective mass spectrum, Poisson scaling and mean centering. The raw intensity at each mass in each pixel is influenced by the topography of the surface and by the secondary ion yield (i.e. matrix effects) therefore it is necessary to pre-process the raw data before PCA in order to cancel bias related to these effects [28]. Details for PCA and data fusion have been reported elsewhere [14,29].

3. Results and discussion

Before charging the sample, the microstructure has been characterized by SE and SI imaging. The ferrite and austenite phases have easily been differentiated by the respective Ni and Cr characteristic signals in ToF-SIMS (lower Cr^+ and higher Ni^+ secondary ion yields indicate austenitic grains) and, alternatively, by EBSD. Previous studies revealed a correlation between EDS elemental and SI image analysis [19].

3.1. Deuterium distribution in ferrite and austenite

ToF-SIMS images of a DSS sample after charging are shown in Fig. 1. At −120 °C, the γ-austenite grains in the microstructure exhibit significantly higher D^- secondary ion yields, indicating a higher D solubility in this phase as compared to the δ-ferrite and a lower diffusivity, respectively. This observation is consistent with the well-known about five orders of magnitude higher diffusivity of D in the δ-ferrite and respectively lower solubility than the austenite phase [30,31].

During slow warm-up of the sample from −120 °C up to room temperature the clear interface between the ferrite and the austenite was blurring (Fig. 1) since the difference in deuterium concentration between ferrite and austenite equilibrates. It is assumed that the deuterium is outgassing directly from the ferrite and austenite grains on the surface whereas the deuterium that is dissolved deeper in the microstructure is released mainly through the ferrite due to the higher diffusion coefficient in this phase. It can be concluded that although the ferrite is acting as a preferred pathway for the effusion and outgassing of deuterium from the (saturated) deeper microstructure [32], the intensity is kept

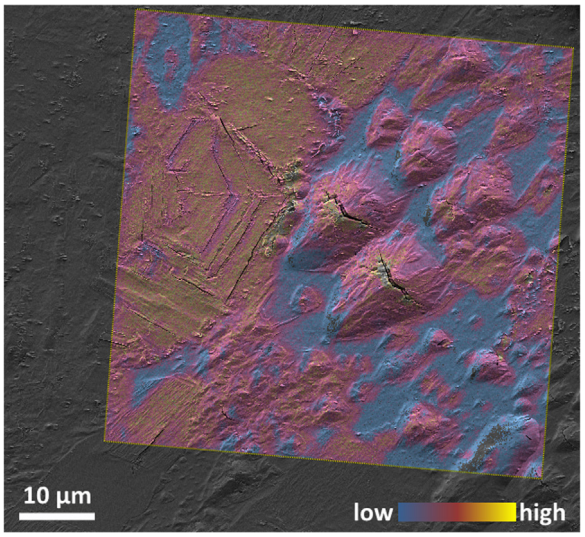

Fig. 2. Fusion of a SEM topographic image and a SIMS PC1 loadings plot representing deuterium in the microstructure (colored). The image reveals needle shaped microtwins in the ferritic phase which are oriented along the grains. The concentration of deuterium is higher in the microtwins as in the ferrite phase surrounding it. The highest concentrations of deuterium is concluded around the cracks. SIMS image data was acquired after 96 h of electrochemical charging. (For interpretation of the references to color in this figure legend, the reader is referred to the web version of this article.)

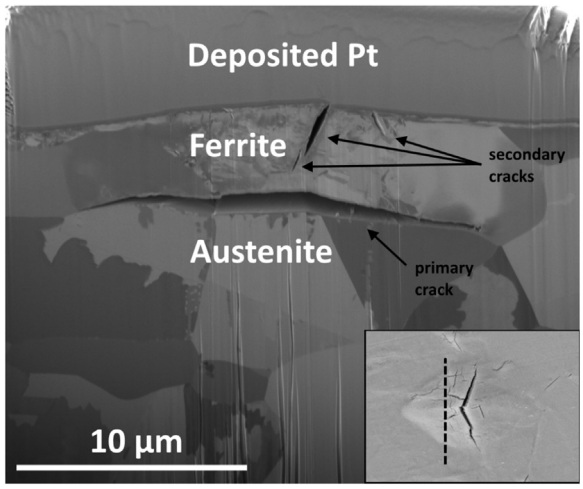

Fig. 3. Total SI image of a FIB cross section normal to a micro-crack observed on the surface of the charged DSS sample. The FIB cut was taken from a different area on the sample than the one displayed in Fig. 2. The FIB cut position is shown in the inset. A separation along the interface between the phases is clearly visible. The inner pressure in the blister caused the formation of secondary cracks in the ferrite. The deposited Pt layer is necessary for FIB and the phase characterization was done by EDS.

relatively low due to the low solubility of deuterium in this phase. It should be emphasized that the term distribution is commonly used in the literature for this effect [8,13,30] although it refers to a faster effusion of deuterium through the ferrite i.e. along the fast pathway. This effect was recently also been anticipated by Mente et al. [33] during finite element modeling of hydrogen assisted cracking in DSS. As confirmed by the ToF-SIMS imaging here, a significant higher mobility of deuterium atoms obviously occurs above ca. −58 °C.

3.2. Deuterium induced twinning and cracking in the ferrite

The deuterium permeation and mechanical properties are different in both phases [34] and thus, it has to be anticipated that also the related cracking behavior differs. The effects of deuterium charging are thus highlighted for each phase separately. By SIMS at a sub-micrometer resolution and data fusion with the respective SEM topography, as described in the previous section, Fig. 2 reveals multiple arrow-head shaped plates. The arrow-head shaped plates were slightly elevated from the ferrite surface having microscale twins at the surface region of the plate. This phenomenon has also been reported in Lublinska et al. [35] for a similar DSS where the formation of hydrogen induced microtwins has been analyzed with light and electron microscopy and with X-ray diffraction as well. As it becomes visible by the respective data fusion, these plates are characterized by a significantly higher concentration of deuterium, as compared to the surrounding ferrite. Particularly at the surface of larger plates, cracks appeared are associated with pronounced accumulations of deuterium around them, as it also becomes evident by Fig. 2. In a series of experiments, it turned out that shorter charging times result in smaller number of plates on the surface in smaller size distribution where on some of the plates no cracks were observed as it was also described by Glowacka et al. [36]. By the EBSD investigations, it turned out that micro-twins have been formed preferentially on the outermost surface of the charged DSS sample. Lublinska [9] and Szummer [11] observed a very similar behavior of ferritic stainless steel microstructures, i.e., the formation of grain oriented needle-shaped plates in the surface layer after electrochemical charging with hydrogen, which can also be taken as another evidence for the similarities in the micro-structural effects caused by hydrogen and deuterium. To elucidate further the observed arrow-head shaped plates at the surface to the microstructure underneath it, focused ion beam (FIB) milling has been utilized to produce a cross section normal to the surface and across one of those features which have been previously been imaged by ToF-SIMS from the topside. Fig. 3 shows a SI image of such FIB preparation which reveals a significant separation at the interface of the grains which was identified by additional EDS analysis as a respective austenite-ferrite interface. Since the grain at the surface has been identified as ferrite, it can be assumed that during charging deuterium has quickly diffused through this phase and subsequently been trapped (and recombined) at the mentioned interface forming these blisters, in particular, because the diffusion coefficient in the underneath lying austenite grain is significantly lower. Base on that it can be assumed that the blister size and the occurring crack along the blister are strongly related to the thickness of the ferrite phase in the surface. Therefore a thinner ferrite region might lead to bigger blisters and in a larger amount. It is anticipated that these high deuterium accumulations then caused or at least contributed to the phase separation at the interface resulting in the respective blistering. It also has to be anticipated that such blistering further strained the ferrite grain above which has been fully saturated and respectively been degraded by deuterium. Since the highest deuterium accumulations have been detected by ToF-SIMS in cracked regions as compared to the surrounding regions in the ferrite (as shown in Fig. 2 by the yellow regions compared to the surrounding areas colored in purple), it cannot be excluded that such deuterium saturation in the ferrite phase also initiated micro-strains, as reported by Tien et al. [29], for instance.

3.3. Deuterium induced twinning, phase transformation and cracking in the austenite

Fig. 4 shows the data fusion of SEM SE topography data with the SIMS image data treated by PCA. Fig. 4a and b are showing the same information although the heat color palette used in Fig. 4a is replaced by a single color where the D concentration is

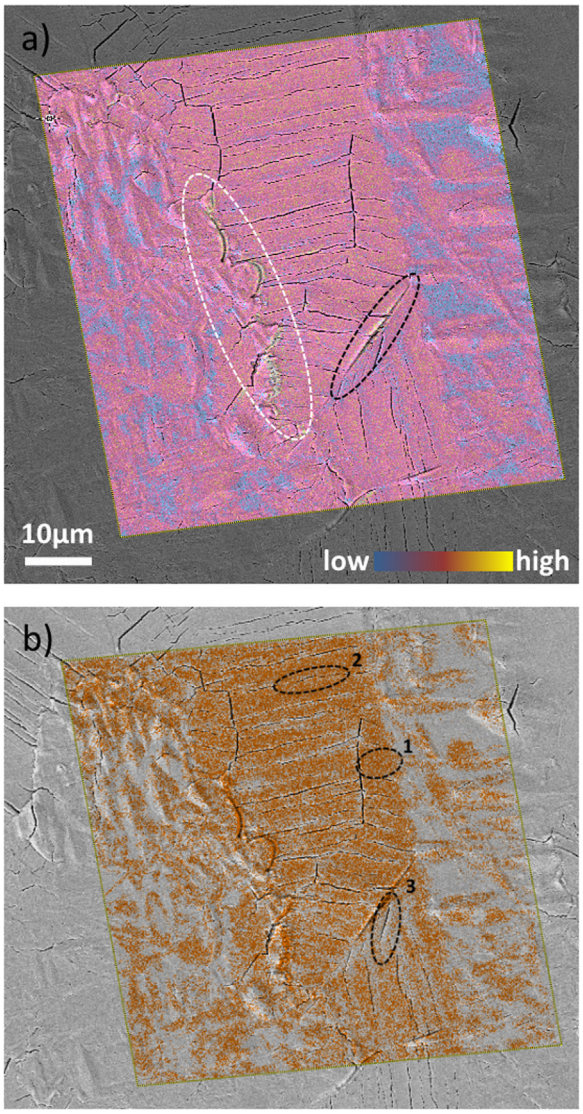

Fig. 4. Fusion of a SEM topographic image and a SIMS PC1 loadings plot representing deuterium in the microstructure (colored). The highest deuterium concentration was observed around some of the parallel cracks and more significantly around larger cracks marked by a black dashed ellipse in (a) and around cracks at the phase boundaries (marked by a white dashed ellipse in (a). Regions 1–3 in (b) are discussed in text and are indicating on three levels of deuterium concentration in the austenite in cracked and non-cracked areas.

represented by the density of colored pixels. Major cracks in the austenite phase can be identified where the respective deuterium concentration indicated by the warmer colors is respectively higher than in the surrounding areas. From this image, significant parallel cracking can be observed in the austenite phase. Such phenomenon associated with deuterium saturation of the austenitic phase has already been reported previously [37]. It has also been observed by Minkovitz, Rozenak and Eliezer [38,39] utilizing diffraction methods (X-ray and TEM) to provide some evidence for a phase transformation caused by electrochemical hydrogen charging and respective crack initiation and propagation in the induced martensitic phase at room temperature. Glowacka et al. [10] also showed the presence of parallel bcc laths inside the austenitic phase indicating that a phase transformation of the austenite into martensite occurs under the presence of hydrogen. The formation of a thin martensite layer on the austenite related to hydrogen was also reported previously by Narita [40] who suggested a transformation sequence of:

$$\gamma \rightarrow \gamma^* \rightarrow \varepsilon$$

where γ is austenite, γ^* is a hydrogen-rich FCC phase formed as a result of the γ lattice expansion and ε is the hydrogen induced martensite phase.

Similarly to the ferritic phase, it can be assumed that high deuterium concentrations cause internal strain in the austenitic grains which lead to an increasing number of stacking faults potentially followed by twinning. Higher deuterium concentrations then lead to formation of ε-martensite on the surface and parallel cracks in the austenite underneath the martensite. Transformation induced martensite (hexagonal close packed, HCP) on the surface of the austenitic phase has been verified by respective SEM/EBSD analysis (as shown in Fig. 5). It turned out that such transformation preferentially occurs where the $\gamma(111)$ planes are perpendicular to the surface, enabling a transformation of a thin layer along $\varepsilon(0001)$. However, cracking associated with deuterium charging of the austenite in the DSS has not only been observed in this predominantly parallel occurrence. Actually, three different regions have been identified in the austenite phase of the investigated DSS that have to be attributed to the various deuterium concentrations (Fig. 4b).

The first region is represented by non-cracked areas with elevated deuterium concentration (marked by #1 in the Fig. 4b). The increased deuterium levels are attributed to non-affected ferrite and, in particular, to the higher solubility of deuterium in the austenite in general. The second region is marked by #2 in Fig. 4b. It occurs around the parallel cracks mentioned above and is characterized by relatively high concentrations of deuterium. The relatively high deuterium concentration in this region can be attributed to the formation of high strains (as in the ferrite) where the deuterium is deeply trapped and/or even to the formation of a deuterium saturated γ^* phase. The third region, marked by #3 in Fig. 4b, has been observed around cracks with relatively low concentrations of deuterium. Here it can be assumed that the lower solubility for deuterium in comparison to austenite is due to a phase transformation into a BCC phase with low deuterium solubility, such as ε. The cracks that have been obtained along the ferrite-austenite interface are attributed to the high deformation of the phases due to charging. The deuterium induced microcracks and the plastic deformation of the surface due to blistering in the ferrite together with parallel cracking and the phase transformation in the austenite were sufficient to cause cracks alongside the interface. A theoretical model proposed by San Marchi [41] has shown that when an external load is applied, a crack can propagate through the austenite by the formation of cleavage micro-cracks in the ferrite, another possibility is that the crack can grow along the interface until it links all the cleavage cracks in the ferrite. Mente et al. [42] discussed the crack path in these two cases by finite element modeling. In the case presented here it can be assumed that the cracks along the interfaces are distributed randomly (as it can be seen in Fig. 4) because no external load was applied. In addition, it cannot be denied that the cracks and the deuterium induced phase transformation in the austenite are not only due to the diffusion of deuterium into the material during charging but also occurring during the effusion and outgassing of deuterium from the sample thereafter as it was shown by Yang et al. [43]. It must be noted that during charging the sample was losing the mirror quality of the polished surface already after 24 h. Therefore it is assumed that most of the changes occurred during charging.

4. Conclusions

ToF-SIMS imaging together with appropriate data treatment

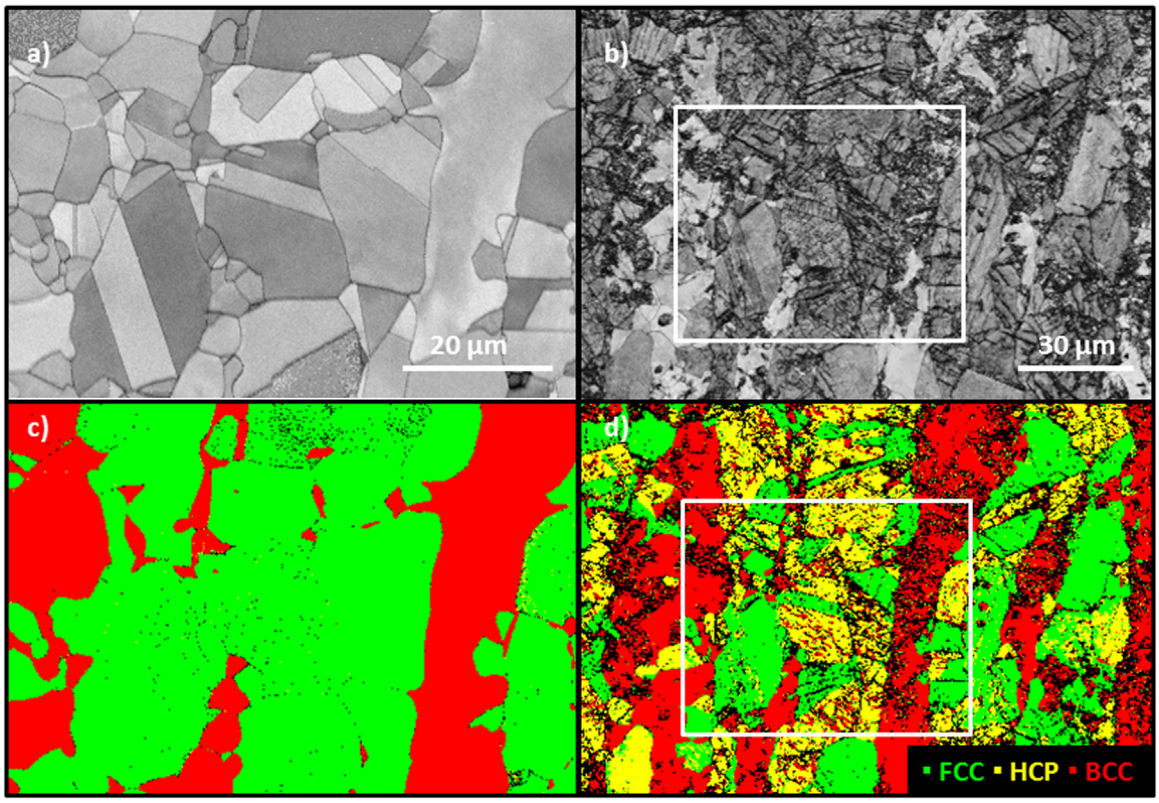

Fig. 5. SE topographic and EBSD phase maps of the sample before (a and c) and after (b and d) charging with deuterium. The area shown in a and c is marked by a white rectangle in b and d. The changes of the surface are caused by charging.

turned out as a strong tool for understanding the interaction of hydrogen and deuterium with a dual phase metal microstructure, like a DSS, visible. The novel procedure of fusing the data delivered by topographic and ToF SIMS chemical imaging for such investigations can be regarded as a significant step beyond the current state of the art for making deuterium and hydrogen interactions visible. The use of a temperature controlled device for the respective deuterium analysis represents a meaningful tool to account for the different diffusion coefficients of deuterium and its solubility in the austenite and the ferrite. The following conclusions can be drawn regarding metallurgical features and specifics of DSS with respect to the deuterium behavior:

- Under UHV conditions, an activation of deuterium in the DSS microstructure appears dependent on temperature. At temperatures below ca. – 60 °C (here −58 °C), most of the charged deuterium is solute in the austenite. Above −60 °C it is increasingly activated and starts to diffuse into the ferrite regions which, at the same time, represent faster diffusion paths, due to diffusivity, and get quickly saturated, also due to their lower solubility, as compared to austenite.
- Ferrite grains in the top layer will thus provide fast diffusion paths for deuterium which then might be trapped at the grain boundary underneath, in particular, if this represents an austenite-ferrite interface. This at least partly might result in blistering at the interface. The arrow-head shaped regions on the surface of the ferrite grains have to be regarded also as a consequence of the blistering and respective deuterium embrittlement of the ferritic micro-structure, notwithstanding the deformation (localized strains) resulting from the blistering underneath.
- Extensive twinning and martensitic phase transformation induced by deuterium in the austenite phase has been observed. This is predominantly followed by parallel cracking of the austenite phase and could be identified by accumulated high deuterium concentrations.
- As further appearance, cracking at the interface between austenite and ferrite has been observed. As has been shown elsewhere [41,42] these might be attributed to high stresses induced, in this case, by charging and distortion of the surface of the phases from both sides of the interface.
- Since no external mechanical load has been applied onto the investigated specimens so far, the always associated accumulation of deuterium around the cracks in the ferrite and the austenite as well indicate that the cracks occurred due to high localized strains in the microstructure introduced by deuterium itself.

Competing financial interests

The author(s) declare no competing financial interests.

Acknowledgements

The authors would like to thanks M. Lagleder for assisting with sample preparation, R. Saliwan Neumann for EBSD-measurements, R. Hesse for FIB measurements, and S. Benemann for the assistance in HR-SEM and EDS image acquisition.

References

[1] I. Alvares-Armas, Recent Pat. Mech. Eng. 1 (2008) 51–57.
[2] R.N. Gunn, Duplex Stainless Steel: Microstructure, properties and Applications, Elsevier, 1997.
[3] M.B. Whiteman, A.R. Troiano, Corrosion 21 (1965) 53–56.

[4] I.M. Robertson, P. Sofronis, A. Nagao, M.L. Martin, S. Wang, D.W. Gross, K.E. Nygren, Metall. Mater. Trans. A – Phys. Metall. Mater. Sci. 46A (2015) 2323–2341.
[5] M. Dadfarnia, P. Novak, D.C. Ahn, J.B. Liu, P. Sofronis, D.D. Johnson, I.M. Robertson, Adv. Mater. 22 (2010) 1128–1135.
[6] T. Mente, T. Boellinghaus, Weld. World 58 (2014) 205–216.
[7] E. Dabah, V. Lisitsyn, D. Eliezer, Mater. Sci. Eng. A – Struct. Mater. Prop. Microstruct. Process. 527 (2010) 4851–4857.
[8] T. Tanaka, K. Kawakami, S.-i Hayashi, J. Mater. Sci. 49 (2014) 3928–3935.
[9] K. Lublinska, A. Szummer, K.J. Kurzydlowski, Hydrogen Induced Microtwins in Cr Alloyed Ferrite, in: B. Baranowski, S.Y. Zaginaichenko, D.V. Schur, V.V. Skorokhod, A. Veziroglu (Eds.) Carbon Nanomaterials in Clean Energy Hydrogen Systems, 2008, pp. 757–764.
[10] A. Glowacka, M.J. Wozniak, G. Nolze, W.A. Swiatnicki, Hydrogen induced phase transformations in austenitic-ferritic steel, in: L. Dobrzynski, K. Perzynska (Eds.) Materials in Transition, Proceedings, 2006, pp. 133-139.
[11] A. Szummer, E. Jezierska, K. Lublinska, J. Alloy. Compd. 293 (1999) 356–360.
[12] O. Sobol, F. Straub, T. wirth, G. Holzlechner, T. Boellinghaus, W.E.S. Unger, Sci. Rep. – Uk 6 (2016).
[13] Z. Tarzimoghadam, M. Rohwerder, S. Merzlikin, A. Bashir, L. Yedra, S. Eswara, D. Ponge, D. Raabe, Acta Mater. 109 (2016) 69–81.
[14] O. Sobol, G. Holzlechner, M. Holzweber, H. Lohninger, T. Boellinghaus, W.E. S. Unger, Surf. Interface Anal. 48 (2016) 474–478.
[15] W.E.S. Unger, V.D. Hodoroaba, Surface Chemical Analysis at the Micro-and Nanoscale, Springer, Berlin, 2013.
[16] T. Awane, Y. Fukushima, T. Matsuo, Y. Murakami, S. Miwa, Int. J. Hydrog. Energy 39 (2014) 1164–1172.
[17] A. Nishimoto, M. Koyama, S. Yamato, Y. Oda, T. Awane, H. Noguchi, ISIJ Int. 55 (2015) 335–337.
[18] M. Kubicek, G. Holzlechner, A.K. Opitz, S. Larisegger, H. Hutter, J. Fleig, Appl. Surf. Sci. 289 (2014) 407–416.
[19] F. Straub, T. Wirth, A. Hertwig, V.D. Hodoroaba, W.E.S. Unger, T. Bollinghaus, Surf. Interface Anal. 42 (2010) 739–742.
[20] Y. Fukai, Met.-Hydrog. Syst. – Basic Bulk. Prop. (1993).
[21] K. Takai, Y. Chiba, K. Noguchi, A. Nozue, Metall. Mater. Trans. A – Phys. Metall. Mater. Sci. 33 (2002) 2659–2665.
[22] C.S. Marchi, B.P. Somerday, S.L. Robinson, Int. J. Hydrog. Energy 32 (2007) 100–116.
[23] K. Takai, J. Seki, Y. Homma, Mater. Trans. JIM 36 (1995) 1134–1139.
[24] P. Kesten, A. Pundt, G. Schmitz, M. Weisheit, H.U. Krebs, R. Kirchheim, J. Alloy. Compd. 330 (2002) 225–228.
[25] E. Owczarek, T. Zakroczymski, Acta Mater. 48 (2000) 3059–3070.
[26] H.H. Johnson, Met. Trans. B 19 (1988) 691–707.
[27] G. Holzlechner, M. Kubicek, H. Hutter, J. Fleig, J. Anal. Spectrom. 28 (2013) 1080–1089.
[28] D.J. Graham, D.G. Castner, Biointerphases 7 (2012) 10.
[29] H. Lohninger, J. Ofner, Spectroscopy Europe 26 (2014) 5.
[30] R. Oltra, C. Bouillot, Hydrog. Transp. Crack. Met. (1994) 17–26.
[31] R. Oltra, C. Bouillot, T. Magnin, Scr. Mater. 35 (1996) 1101–1105.
[32] A. Turnbull, R.B. Hutchings, Mater. Sci. Eng. A – Struct. Mater. Prop. Microstruct. Process. 177 (1994) 161–171.
[33] T. Mente, T. Boellinghaus, Weld. World 56 (2012) 66–78.
[34] V. Olden, C. Thaulow, R. Johnsen, Mater. Des. 29 (2008) 1934–1948.
[35] K. Lublinska, A. Szummer, K.J. Kurzydlowski, 17th European Conference on Fracture, Brno, Czech Republic, 2008.
[36] A. Glowacka, W.A. Swiatnicki, J. Alloy. Compd. 356 (2003) 701–704.
[37] F. Straub, T. Boellinghaus, W.E.S. Unger, T. Mente, International Hydrogen Conference (IHC 2012), ASME Press, 2012, pp. 505–513.
[38] E. Minkovitz, D. Eliezer, J. Mater. Sci. Lett. 1 (1982) 192–194.
[39] P. Rozenak, D. Eliezer, Metall. Trans. A – Phys. Metall. Mater. Sci. 19 (1988) 723–730.
[40] N. Narita, C.J. Altstetter, H.K. Birnbaum, Metall. Trans. A – Phys. Metall. Mater. Sci. 13 (1982) 1355–1365.
[41] C.S. Marchi, B.P. Somerday, J. Zelinski, X. Tang, G.H. Schiroky, Metall. Mater. Trans. A – Phys. Metall. Mater. Sci. 38a (2007) 2763–2775.
[42] T. Mente, T. Boellinghaus, Numerical investigations on hydrogen-assisted cracking in duplex stainless steel microstructures, in: T. Boellinghaus, J. C. Lippold, C.E. Cross (Eds.), Cracking Phenomena in Welds IV, Springer, 2016, pp. 329–359.
[43] Q. Yang, J.L. Luo, Mater. Sci. Eng. A – Struct. Mater. Prop. Microstruct. Process. 288 (2000) 75–83.